Waterlike glass polyamorphism in a monoatomic isotropic Jagla model

Limei Xu,[1,2,a)] Nicolas Giovambattista,[3] Sergey V. Buldyrev,[4] Pablo G. Debenedetti,[5] and H. Eugene Stanley[6]
[1]*WPI-AIMR, Tohoku University, Sendai, Miyagi 980-8577, Japan*
[2]*International Center for Quantum Materials, Peking University, Beijing 100871, China*
[3]*Department of Physics, Brooklyn College of the City University of New York, Brooklyn, New York 11210, USA*
[4]*Department of Physics, Yeshiva University, New York, New York 10033, USA*
[5]*Department of Chemical and Biological Engineering, Princeton University, Princeton, New Jersey 08544-5263, USA*
[6]*Center for Polymer Studies and Department of Physics, Boston University, Boston, Massachusetts 02215, USA*

(Received 20 July 2010; accepted 8 November 2010; published online 9 February 2011)

We perform discrete-event molecular dynamics simulations of a system of particles interacting with a spherically-symmetric (isotropic) two-scale Jagla pair potential characterized by a hard inner core, a linear repulsion at intermediate separations, and a weak attractive interaction at larger separations. This model system has been extensively studied due to its ability to reproduce many thermodynamic, dynamic, and structural anomalies of liquid water. The model is also interesting because: (i) it is very simple, being composed of isotropically interacting particles, (ii) it exhibits polyamorphism in the liquid phase, and (iii) its slow crystallization kinetics facilitate the study of glassy states. There is interest in the degree to which the known polyamorphism in glassy water may have parallels in liquid water. Motivated by parallels between the properties of the Jagla potential and those of water in the *liquid* state, we study the metastable phase diagram in the *glass* state. Specifically, we perform the computational analog of the protocols followed in the experimental studies of glassy water. We find that the Jagla potential calculations reproduce three key experimental features of glassy water: (i) the crystal-to-high-density amorphous solid (HDA) transformation upon isothermal compression, (ii) the low-density amorphous solid (LDA)-to-HDA transformation upon isothermal compression, and (iii) the HDA-to-very-high-density amorphous solid (VHDA) transformation upon isobaric annealing at high pressure. In addition, the HDA-to-LDA transformation upon isobaric heating, observed in water experiments, can only be reproduced in the Jagla model if a free surface is introduced in the simulation box. The HDA configurations obtained in cases (i) and (ii) are structurally indistinguishable, suggesting that both processes result in the same glass. With the present parametrization, the evolution of density with pressure or temperature is remarkably similar to the corresponding experimental measurements on water. Our simulations also suggest that the Jagla potential may reproduce features of the HDA-VHDA transformations observed in glassy water upon compression and decompression. Snapshots of the system during the HDA-VHDA and HDA-LDA transformations reveal a clear segregation between LDA and HDA but not between HDA and VHDA, consistent with the possibility that LDA and HDA are separated by a first order transformation as found experimentally, whereas HDA and VHDA are not. Our results demonstrate that a system of particles with simple isotropic pair interactions, a Jagla potential with two characteristic length scales, can present polyamorphism in the glass state as well as reproducing many of the distinguishing properties of *liquid* water. While most isotropic pair potential models crystallize readily on simulation time scales at the low temperatures investigated here, the Jagla potential is an exception, and is therefore a promising model system for the study of glass phenomenology. © *2011 American Institute of Physics*. [doi:10.1063/1.3521486]

I. INTRODUCTION

Monoatomic liquids with isotropic interactions usually exhibit simple thermodynamic behavior,[1] in contrast to network-forming systems such as water,[2] silica,[3] or silicon.[4] It had long been believed that in order for a liquid to have complex, waterlike properties such as negative thermal expansion, it is necessary for it to possess the key feature of anisotropic interactions. Forty years ago, Hemmer and Stell[5,6] showed that monoatomic systems interacting via core-softened pair potentials can show structural transitions in the solid phase. These pair potentials are characterized by a repulsive hard core part decorated by a shoulder or ramp that "softens" the repulsion between atoms at very short distances [see, e.g., Fig. 1(a)]. Numerous subsequent studies have shown that core-softened potentials can exhibit a range of anomalous properties,[7] such as density or diffusion anomalies, that are known to occur in water[8–13] and liquid metals.[14–16] It is now understood that anisotropic interactions, such as hydrogen bonds, are not necessary for a liquid to have anomalous, waterlike properties[17] and that core-softened potentials

a)Author to whom correspondence should be addressed. Electronic mail: limei.xu@wpi-aimr.tohoku.ac.jp.

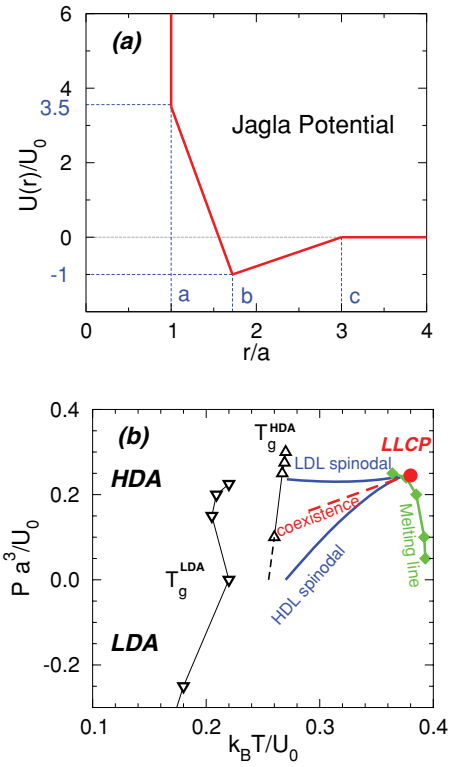

FIG. 1. (a) The spherically-symmetric two-scale Jagla potential with attractive and repulsive ramps. Here a is the hard-core diameter, $b = 1.72a$ is the soft-core diameter, and $c = 3a$ is the long distance cutoff. (b) Phase diagram of a system of particles interacting with the Jagla potential (Ref. 19). We indicate LDL and HDL spinodal lines (solid blue). The LDL-HDL coexistence (dashed red) line ends in a liquid-liquid critical point. T_g are the glass transformation temperatures of HDA (up triangles) and LDA (down triangles). We also indicate the melting line of the hcp crystal (solid green line with rhombi). We calculate T_g based on the computational equivalent of the differential scanning calorimetry method: (i) obtain the isobaric specific heat $C_p(T)$ upon heating the glass, and (ii) obtain T_g based on $C_p(T)$ following the procedure of Ref. 19. We use a heating rate of 10^{-5} q_0 for HDA and a faster heating rate of 8.9×10^{-4} q_0 for LDA to avoid crystallization. The nonmonotonic behavior of the LDA glass transition temperature with pressure is related to the diffusion anomaly (increase of diffusivity upon compression) of the Jagla LDL which exists in the region of positive pressures and low temperatures (Ref. 22).

can serve as coarse-grained models of more complex molecular systems,[18] and are good model systems for studying the thermodynamics of waterlike anomalies in general.[19] Recently, a different type of monoatomic model for water, which includes a three-body (anisotropic) interaction, has been introduced that reproduces many of the structural, dynamic and thermodynamic properties of water.[20]

One of the most interesting properties of core-softened potentials is the fact that they can show polyamorphism, i.e., the presence of two or more liquid or glassy states.[8,21,22] The concept of polyamorphism is relatively new. This phenomenon was first demonstrated in *glassy* water,[23,24] and was subsequently proposed for *liquid* water[25] and partially tested for *bulk*[26,27] and *confined* water[28] and observed in other substances such as phosphorous,[29] germanium,[30] the liquid metal $Ce_{55}Al_{45}$,[31] triphenyl-phosphite,[32] and in yttrium oxide-aluminum oxide melts [$(Al_2O_3)_{1-x}(Y_2O_3)_x$ with $x \approx 0.20$].[33–35] A helpful recent review is Ref. 36.

An example of a core-softened potential that exhibits polyamorphism is shown in Fig. 1(a). The phase diagram for this model system [Fig. 1(b)][22,37] includes two liquid phases separated by a first-order transition line, which ends in a liquid-liquid critical point (LLCP). This LLCP, unrelated to the liquid-gas critical point, is located above the glass transition temperature $T_g(P)$ and the melting temperature $T_m(P)$, and can therefore be studied in equilibrium simulations.[22] The two liquids, referred to as low-density liquid (LDL) and high-density liquid (HDL), transform to low-density amorphous (LDA) and high-density amorphous (HDA) solids upon fast isobaric cooling.[19]

Most studies of core-softened potential systems have focused on the liquid state. Little attention has been paid to the behavior of these model systems in the glassy state, and to comparing simulation results to experiments. A probable reason underlying this situation is the fact that atomic systems with isotropic interactions crystallize easily in computer simulations, even when the accessible simulation time scales are several orders of magnitude shorter than those employed in experiments. The Jagla pair potential of Fig. 1(a) is an exception, and the corresponding system can be studied in the deeply supercooled state using molecular dynamics simulations.[19] To our knowledge, there is no systematic study to date based on molecular dynamics (MD) simulations that investigates the extent to which monodisperse systems of particles interacting via core-softened potentials are able to reproduce vitreous polyamorphism, such as is observed experimentally.

Jagla used a Monte Carlo (MC) simulation to systematically investigate the low temperature behavior of models of the general form of that shown in Fig. 1(a), both with and without an attractive ramp, in both two and three dimensions.[8] Of particular relevance to this work, he studied the influence of attractions on low-temperature phase behavior, including the appearance of an LDL-HDL polyamorphic transition terminating at a LLCP. In this work, we extend Jagla's investigations at low temperatures and explore all amorphous-amorphous and crystal-amorphous transformations known to occur in water.

In actual experiments, compression/decompression and cooling/heating rates can play a crucial role. Our choice of using MD instead of MC simulations is motivated by the fact that time, and hence compression/decompression and cooling/heating rates, are well-defined in the MD case. This allows us to compare different transformations obtained in simulations under similar computational protocols. For example, we can compare how the low-pressure glass and the low-pressure crystal evolve upon compression when the *same* compression rate is used.

The phenomenology of water in the glass state is very rich (for a helpful review, see Ref. 38). When the low-pressure stable ice (ice I_h) is compressed at $T = 77$ K, it transforms to a HDA ice above $P \approx 1$ GPa.[23] If HDA is decompressed at the same temperature and then heated at $P = 1$ bar, it transforms abruptly to LDA ice, at $T \approx 117$ K.[23] LDA and HDA can be interconverted upon compression and decompression at $T \approx 135$ K.[39] A third amorphous state, called very-high-density amorphous (VHDA) ice, has been proposed

to exist at $P > 1$ GPa and $T > 130$ K.[38,40] In this work, we study these transformations using discrete-event molecular dynamics simulations[41] of a system of particles interacting via the pair potential shown in Fig. 1(a). For this parametrization, a quantitative comparison of calculated (P,T,ρ) values with experimental data for liquid water is possible (see Ref. 18), and here we extend this comparison to the glass state.

We present simulation details in the next section and we describe the pressure-induced amorphization of the low-pressure crystal in Sec. III. We study the transformations between the LDA and HDA forms of the Jagla potential in Sec. IV and the formation of VHDA at high pressure in Sec. V, where we also compare the HDA-LDA and the VHDA-HDA transformations during isotropic stretching simulations. We present conclusions and suggestions for further investigation in Sec. VI.

II. SIMULATIONS

Our results are based on discrete-event MD simulations[14,37,41–43] of a system composed of $N = 1728$ particles interacting via the discretized version of the Jagla potential shown in Fig. 1(a). This pair potential is characterized by two length scales,[8] a hard-core distance $r = a$ and a soft-core distance $r = b = 1.72a$. The attractive part of the pair potential extends up to $r = c = 3a$ and has a minimum energy $-U_0$.

All quantities reported in this work are in reduced units. Distances and energies are in units of a and U_0, respectively. Time, t, is calculated in units of $a\sqrt{m/U_0}$, where m is the particle mass. The density $\rho \equiv N/L^3$, is calculated in units of a^{-3}. Pressure units are U_0/a^3 and temperature units are U_0/k_B.

We perform simulations at constant pressure and temperature. During the isothermal compression/decompression simulations, we increase/decrease the pressure by ΔP each time interval Δt. The compression/decompression rates are $q_P \equiv \Delta P/\Delta t$. We calculate q_P in units of $q_P^0 \equiv a^{-4}\sqrt{U_0^3/m}$. Similarly, for the isobaric cooling/heating simulations, we increase/decrease the temperature by ΔT each time interval Δt, the cooling/heating rate being $q_T \equiv \Delta T/\Delta t$. We calculate q_T in units of $q_T^0 \equiv a^{-1}k_B^{-1}\sqrt{U_0^3/m}$. The compression/decompression and cooling/heating rates can be related to experimental situations upon assigning the following values to a, U_0 and m:[18]

- $a = 0.27$ nm (the position of the first peak of the oxygen-oxygen pair correlation function in water),
- $U_0 = 4.75$ kJ/mol (which assures that the Jagla model has the same value of the maximum temperature of the locus of the maximum density in the T-P plane, $T \approx 285$ K, as that observed in water), and
- $m = 36$ g/mol (since the mass of two water molecules can be identified with the mass of one particle in the Jagla liquid[18]).

As a result, $q_T^0 = 7.7 \times 10^{14}$ K/s and $q_P^0 = 5.4 \times 10^{12}$ kbar/s. This value of q_T^0 implies that the slowest cooling/heating rate used in this work ($= \pm 10^{-5}\, q_T^0$) is of the same order of magnitude as the slowest cooling/heating rate used in the MD simulation of extended simple point charge (SPC/E) water in Ref. 44. Similarly, the resulting value of q_P^0 implies that the slowest compression/decompression rate used in this work ($= \pm 10^{-8} q_P^0$) is approximately 4 orders of magnitude smaller than that used in MD simulation of TIP4P water in Ref. 45.

Although the Jagla potential with the parametrization used in this work exhibits waterlike anomalies, it also has distinctly non-waterlike features. Specifically, the phase diagram of our Jagla potential [Fig. 1(b)] features a coexistence line between LDL and HDL that has a positive slope in the (P, T) plane. In contrast, experimental data and thermodynamic considerations indicate that this slope must be negative for water.[2] An LDL-HDL coexistence line with negative slope can be obtained with the Jagla potential if one uses a different parametrization than the one used here,[21] but this model easily crystallizes above the LLCP critical temperature and therefore is not convenient for studying polyamorphism.

Another distinction between water and the particular parameterization of the Jagla model used here is the fact that the region of density anomaly in water extends to negative pressures, so that the maximum temperature of the locus of maximum densities in water lies in the region of negative pressure. In the Jagla model with the present parameters, in contrast, density anomalies occur only at positive pressures.

III. HIGH-DENSITY AMORPHOUS SOLID FROM LOW-PRESSURE CRYSTAL

In 1984, Mishima *et al.*[23] observed that compressing ice I_h at $T = 77$ K above $P \approx 1$ GPa produces a glass, which is called HDA ice. This was the first time that a glass was formed by pressure-induced amorphization (PIA) of a crystal. PIA of crystals in other substances was observed soon thereafter.[46–53]

In our first set of simulations, we follow the protocol used in the PIA experiments of Ref. 23. Specifically, we compress the low-pressure hcp crystal of the Jagla potential[19] at constant temperature $T = 0.1$. This temperature is well below the glass transition temperature T_g and the melting temperature T_m of the Jagla model.[19]

Figure 2(a) shows the volume of the system $V(P)$ as a function of pressure obtained from our simulations. To obtain the hcp crystal, we slowly cool LDL at constant volume to low temperature $T = 0.1$, and then equilibrate the system for 42 000 time units at the same volume ($L/a = 18.6$) and higher temperature ($T = 0.225$), which results in a better crystal structure. The resulting hcp crystal is further equilibrated for a long time ($t = 50\,000$) at $P = 0.2$, $T = 0.1$ before all the calculations involving hcp are performed. For $P \lesssim 1.25$ to a very good approximation, $V(P)$ decreases linearly with pressure, indicating that the hcp crystal is compressed elastically. We observe a similar behavior at high pressure, $P \gtrsim 1.6$. The abrupt change in volume that occurs at $P \approx 1.35$ corresponds to the transformation of the hcp crystal into an amorphous solid.

The behavior of $V(P)$ obtained in simulations is strikingly similar to the results obtained in experiments for the case of glassy water. Figure 2(b) shows the piston displacement $d(P)$ as a function of pressure for ice I_h samples compressed at $T = 77$ K.[23] The sample undergoes elastic com-

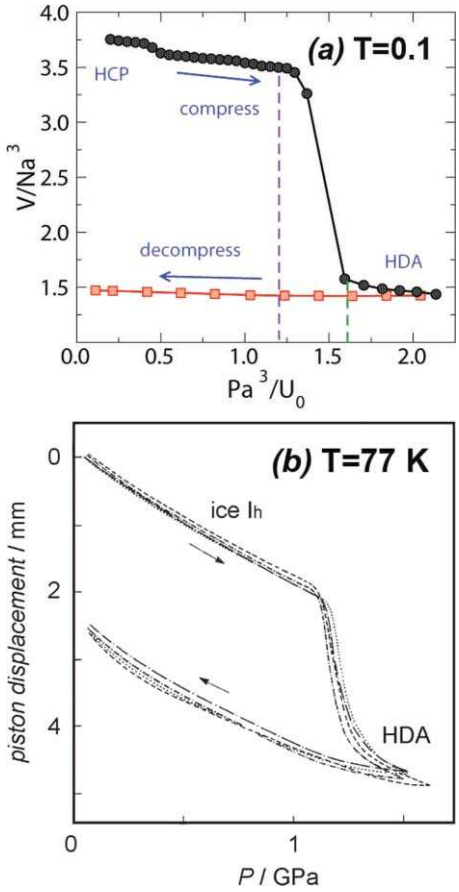

FIG. 2. Crystal-to-HDA transition on compression followed by decompression of HDA. (a) Simulations: Pressurization of hcp crystal at $T = 0.1$ results in HDA (circles). An apparent first-order transition occurs at $P = 1.35$, and is indicated by the sharp drop in volume. The dashed vertical lines indicate the pressures at which the hcp (violet) and HDA (green) radial distribution functions shown in Fig. 3 were obtained. The hcp-to-HDA transition is not reversible as the volume of HDA barely changes upon decompression at the same temperature, $T = 0.1$ (squares). (b) Experiments: Piston displacement as a function of pressure for four samples of ice I_h compressed at $T = 77$ K. The resemblance between panels (a) and (b) is evident. The sample pressure is ≈ 0.9 times the nominal pressure. Adapted with permission from O. Mishima, L. D. Calvert, and E. Whalley, Nature (London) **310**, 393 (1984). Copyright 1984, Nature.

pression while $d(P) \propto P$ at low and high pressures, but $d(P)$ changes suddenly at $P \approx 1.2$ GPa when ice I_h converts to HDA.

In both simulations and experiments, the conversion from the low pressure crystal to the amorphous solid appears to be first-order since $\partial P/\partial V \approx 0$ during the transformation. Moreover, in both cases, the crystal-amorphous solid transformation is not reversible in that the isothermal decompression of HDA solids does not result in ice I_h in actual experiments, nor do simulations recover the hcp crystal.

To test whether the PIA of the hcp crystal indeed results in an amorphous state, we calculate the radial distribution function (RDF), $g(r)$, of the hcp crystal and HDA (Fig. 3). The RDF of the hcp crystal shows clear maxima for large values of r, an indication of long-range order. Instead, the RDF of HDA shows maxima only for $r/a \lesssim 3.2$, indicating that HDA is characterized by short-range order and, thus, has an amorphous structure. Figure 3 also shows that, during the hcp crystal-to-HDA transition, particles separated by a distance

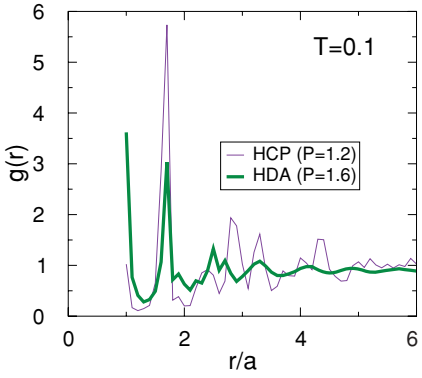

FIG. 3. Demonstration that the structure at $P = 1.6$ is amorphous, while the structure at $P = 1.2$ is crystalline at $T = 0.1$ (see Fig. 2). Radial distribution function, $g(r)$, of hcp at $P = 1.2$ and HDA at $P = 1.6$. During the transition, particles separated by a distance $r/a \approx 1.72 = b/a$, corresponding to the minimum of the pair potential interaction (Fig. 1), move closer to a separation distance $r/a \approx 1$, corresponding to the hard-core of the pair potential interaction. Thus, for any given particle, neighboring particles in the second neighbor shell move toward the first shell upon compression, also resulting in a loss of long-range order, as evidenced by the disappearance of the $g(r)$ maxima when going from $P = 1.2$ (hcp) to $P = 1.6$ (HDA).

$r/a = 1.72 = b/a$, corresponding to the minimum of the pair potential interaction [Fig. 1(a)], move closer to a separation $r/a = 1$, corresponding to the hard-core of the pair potential interaction. The amorphous character of HDA is also confirmed by Figs. 4(a) and 4(b) which show snapshots of the system in the hcp crystal and HDA states, respectively.

IV. TRANSFORMATIONS BETWEEN LOW-DENSITY AND HIGH-DENSITY AMORPHOUS SOLIDS

A. Isobaric heating of recovered high-density amorphous solid

Experiments on water indicate that if HDA is recovered at ambient pressure and $T = 77$ K, and is then heated isobarically, it transforms to an LDA solid at $T \approx 117$ K.[23] This second form of glassy water is structurally similar to the glasses obtained by hyperquenching the liquid at normal pressure (hyperquenched glassy water, HGW) or by vapor deposition on a cold plate (amorphous solid water, ASW).[54–57] In both cases, appropriate annealing is usually required.

We test whether an HDA-to-LDA transformation can be reproduced in simulations using the Jagla potential. To do this, we heat an HDA configuration at $P = 0.1$ until the equilibrium liquid is recovered. The HDA is obtained upon compression of hcp at $T = 0.1$, followed by isothermal decompression down to $P = 0.1$ (Fig. 2). Figure 5 shows the temperature dependence of the volume upon isobaric heating performed at a heating rate $10^{-5}\ q_T^0$. A sharp change in volume occurs in the range $T \approx 0.25-0.35$. It is tempting to associate this change in volume with the HDA-to-LDA transformation. However, we find that at $P = 0.1$ the glass transition temperature of HDA is $T_g^{\mathrm{HDA}}(P) \approx 0.26 \pm 0.01$ [see Fig. 1(b)]. We estimate T_g using the computational equivalent of the "differential scanning calorimetry" procedure, as described in detail in Ref. 19, namely by estimating a crossover point at which the specific heat begins to increase sharply upon heating. We also find that when HDA is an-

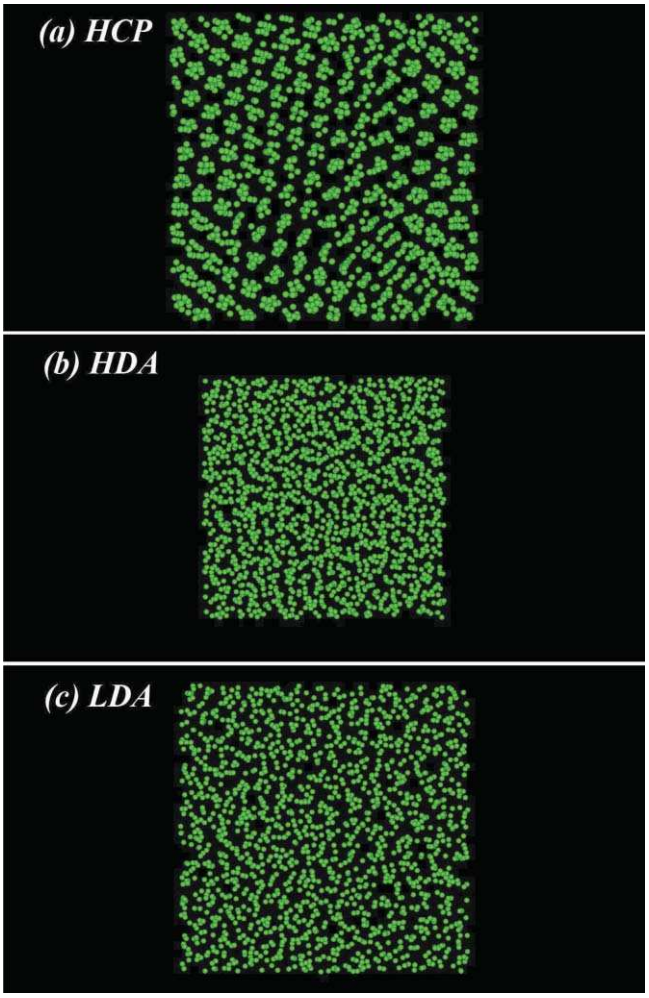

FIG. 4. Snapshots of the system during the hcp-to-HDA transition at $T = 0.1$ (see Fig. 2): (a) hcp ($P = 1.2$) and (b) HDA ($P = 1.6$). (c) Snapshot of the system corresponding to LDA at $T = 0.1$. LDA is obtained upon isochorically quenching the equilibrium liquid followed by long time equilibration at $P = 0.1$ and $T = 0.1$.

nealed at $T = 0.27$ and $P = 0.1$ it transforms to a liquid with a relaxation time of approximately 7000 time units. We estimate the relaxation time as the time at which the root mean square displacement of particles due to diffusion is equal to the hard core diameter a. Note that T_g^{HDA} approximately coincides with the temperature at which the volume starts to change abruptly in Fig. 5. Therefore, the sharp change of volume in Fig. 5 occurs in the liquid phase and thus cannot be related to the HDA-to-LDA transformation. Moreover, since the HDL spinodal line at $P = 0.1$ occurs at $T = 0.3$ [Fig. 1(b)], the system is in the HDL phase over the approximate range $0.26 < T < 0.3$ and in the LDL phase above approximately $T = 0.3$. Interestingly, the slope of the $V(T)$ curve in Fig. 5 changes at $T = 0.3$, i.e., at the temperature at which HDL transforms to LDL.

Note that a necessary condition to find the HDA-to-LDA transition upon isobaric heating is that $T_g^{\mathrm{HDA}}(P) > T_{\mathrm{spinodal}}^{\mathrm{HDL}}(P)$. Figure 1 suggests that this may occur only at $P < 0$, so an HDA-to-LDA transformation may be observable in the present simulations only at negative pressure. The lowest pressure at which we can determine the HDL spinodal is $P = 0.0$ at which the liquid HDL transforms into LDL at

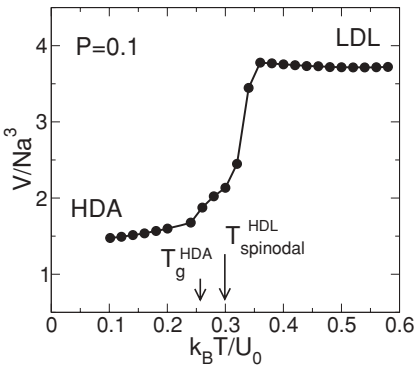

FIG. 5. Volume as a function of temperature as HDA is heated isobarically at $P = 0.1$. HDA is obtained by compressing hcp [see Fig. 2(a)] at $T = 0.1$, followed by isothermal decompression down to $P = 0.1$. HDA converts to HDL at the glass transition temperature $T_g^{\mathrm{HDA}} \approx 0.26$, and HDL converts to LDL at the HDL spinodal temperature $T_{spinodal}^{\mathrm{HDL}} \approx 0.3$.

$T = 0.27$ after 3000 time units while the relaxation time is 400 time units. Note that the $T_g(P)$ line for HDA is quite steep in Fig. 1(b), thus it must cross the HDL spinodal at some pressure between $P = -0.05$ and $P = -0.1$ if we assume, for the purpose of extrapolation, that both the glass transition and the spinodal loci for HDL are linear in the (P, T) plane [see Fig. 1(b)]. The precise determination of their crossing point is not possible at present, because of the large numerical uncertainty in the T_g value ($T_g = 0.26 \pm 0.01$). We attempted to confirm that HDA transforms to LDA at $P < 0$ by aging HDA at $P = -0.25$ and $T = 0.2$, but find that HDA spontaneously transforms into LDL after 10^4 time units. For this pressure, it is impossible to determine T_g for HDA, since the system remains in a glassy state until it transforms into LDL. We confirmed this by calculating the root mean square displacement of particles during HDA aging, and find that this quantity remains less than $0.7a$ during the entire aging process.

For $P < 0.0$, the HDA spinodal is not well defined since the temperature at which HDA transforms to LDL decreases with the decreasing heating rate even at the slowest heating rates we are able to achieve. For example, at $P = -0.25$ and $q = 4 \times 10^{-5}\, q_T^0$ the transformation of HDA into LDL occurs at approximately $T = 0.25 \pm 0.01$ and varies across the HDA samples studied. In contrast, for aging at the same pressure, the transition occurs at $T = 0.2$ as stated above. We make sure that the resulting state is LDL by performing the computational equivalent of differential scanning calorimetry of LDL (see Ref. 19 for details) at $P = -0.25$ which shows that $T_g^{\mathrm{LDA}} \approx 0.18$. We also find that at $P = -0.25$ and $T = 0.2$ the relaxation time in the resulting LDL is 1700 time units. Not surprisingly, the resulting LDL crystallizes into hcp after equilibrating at $T = 0.2$ and $P = -0.25$ for 6000 time units. In this case the slope of the volume versus temperature plot is positive, both for HDA and LDL, since $P = -0.25$ lies below the region of the density anomaly.

To test if HDA may transform directly into LDA upon isobaric heating we perform similar aging simulations at $P = -0.5$. At negative pressures the LDA glass transition temperature drops sharply with pressure [Fig. 1(b)]. In particular, $T_g^{\mathrm{LDA}} = 0.15$ at $P = -0.5$. We find that at these con-

ditions HDA can survive without any noticeable changes for the entire length of our simulations (10^5 time units). At $P = -0.5$, we were able to observe the transformation from HDA to LDL only at $T = 0.18$, after aging the system for 3.4×10^4 time units. The resulting low density phase is clearly in the liquid state (relaxation time is only 100 time units). It is likely that this trend will continue at even lower pressures. Therefore, we conclude that in the Jagla model LDA cannot be obtained from HDA by isobaric heating.

Note, however, that in real experiments with water, the recovered sample of HDA has a free surface in contact with the piston or with the atmosphere, while in computer simulations we use periodic boundary conditions and the system needs to overcome an energetic barrier in order to create an interface between HDA and LDA, which may require much larger negative pressures than the actual transformation between HDA and LDA once the interface is created. In order to verify this hypothesis we perform the additional following simulations. We cut the HDA sample of $N = 1728$ particles and insert into a simulation box a wide slab of vacuum parallel to the xy-plane. After this we perform constant volume simulations, keeping periodic boundary conditions and selecting the $x = 15.5$ and $y = 15.5$ dimensions of the simulation box, which roughly correspond to zero stress in x and y directions. The measured component of the stress tensor in z direction is strictly zero, while the x and y components fluctuate slightly below zero due to the surface tension between different states. We perform recovery simulations at three different temperatures $T = 0.175$, 0.19, and 0.2, all below the LDA glass transition temperature at $P = 0$, which we estimate at $T_g^{\mathrm{LDA}} = 0.22$ [Fig. 1(b)]. To confirm that this estimation is correct we perform constant pressure ($P = 0$) and temperature simulations by quenching bulk LDL. We see that in all three cases the relaxation time is longer than our maximum simulation time 10^5. At $T = 0.175$, we observe the quick formation of two thin (about $4.6a$ in depth) LDA layers on both sides of the HDA slab, which do not grow with time [Fig. 6(a)]. At $T = 0.19$ the LDA layers grow slowly but steadily and we estimate that the complete disappearance of the HDA slab would happen in 3×10^5 time units. This corresponds to a HDA-LDA interface velocity of 2×10^{-5} velocity units ($\sqrt{U_0/m}$). If we use $U_0 = 4.75$ kJ/mol and $m = 0.036$ kg/mol, this velocity is about 7 mm per second. At $T = 0.2$ we observe a complete disappearance of the HDA slab in 2.8×10^4 time units [see Fig. 6(b)], which corresponds to a velocity of interface motion of $1.2 \times 10^{-4}\sqrt{U_0/m}$, or 4.5 cm per second. Recall that Mishima[23] found that HDA, recovered at atmospheric pressure, transforms to LDA at 117 K. This value is equal to $0.86T_g$ if one accepts the LDA glass transition temperature $T_g = 136$ K.[58] In our simulations $0.86T_g = 0.189$, which is in very good agreement with the temperature 0.19 at which we observe slow motion of the HDA-LDA interface.

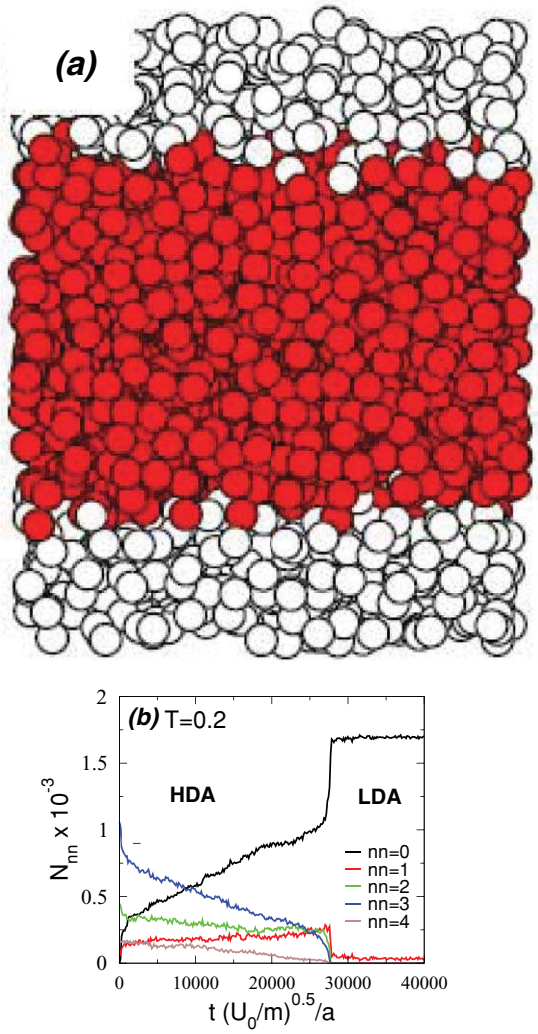

FIG. 6. (a) Snapshot of the system during HDA recovery at $T = 0.175$ taken at 10^4 time units after any change in the system stops. In this simulation, the system is composed of an HDA slab with free surfaces in order to enable the HDA-to-LDA transformation. Particles in the LDA and HDA phases are represented by white and red spheres, respectively. (b) Number of particles with different number of nearest neighbors nn (separated by a distance $r_{ij} < 1.3a$) as function of time during HDA recovery at $T = 0.2$. At this temperature, HDA transforms continuously to LDA and, in this particular simulation run, the system fully transformed to LDA after 2.8×10^4 time steps. In LDA, most particles have ≤ 1 nearest neighbors.

B. Isothermal compression of low-density amorphous solid

Experiments on many substances, such as metallic glasses,[31] water,[23] phosphorous,[29] silicon,[59] triphenyl-phosphite,[60] and yttrium oxide-aluminum oxide melts [$(Al_2O_3)_{1-x}(Y_2O_3)_x$ with $x \approx 20$],[33,35] display polyamorphism.[36] In some of these materials, polyamorphism can be observed in the glassy state and both LDA and HDA can be produced. For example, in the case of water, isothermal compression of LDA (or, alternatively, HGW or ASW) at $T = 77$ K results in HDA at $P \gtrsim 0.6$ GPa.[23,61] Although the LDA-to-HDA transformation is not reversible upon decompression at $T = 77$ K,[23] HDA converts back to LDA if the compression–decompression processes are performed at $T \approx 135$ K.[39] To test whether the LDA-to-HDA transformation can be observed in simulations using the Jagla potential, we first create LDA at low pressure. As discussed in the previous section, we cannot obtain LDA configurations following the experimental procedure (i.e., isobaric heating

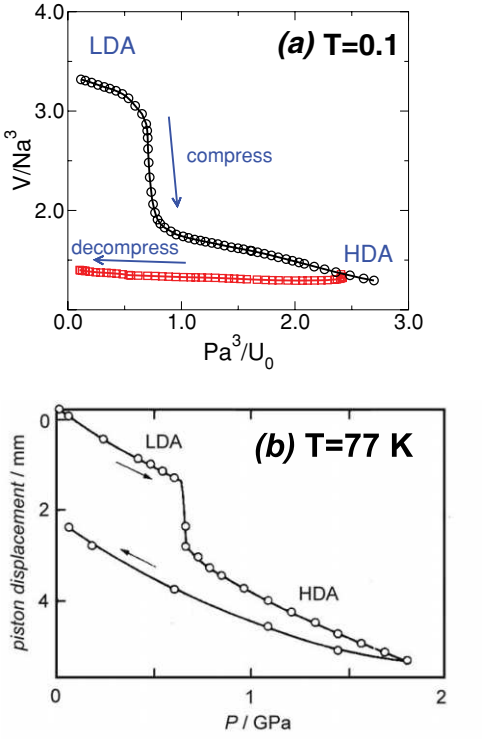

FIG. 7. LDA-to-HDA transformation and subsequent decompression of HDA from (a) simulations using the Jagla potential and (b) water experiments (adapted from Ref. 23). In the simulations, LDA is obtained upon isochorically quenching the equilibrium liquid followed by long time equilibration at $P = 0.1$ and $T = 0.1$. LDA is then compressed at $T = 0.1$ and transformed to HDA at $P \approx 0.7$ (circles), as indicated by the sharp change in volume. The transformation is not reversible at this temperature, as the volume of HDA barely changes upon decompression at $T = 0.1$ (squares). In the experiments (Ref. 23), LDA is obtained by isobaric heating of recovered HDA at zero-pressure above ≈ 117 K. LDA is then cooled back to $T = 77$ K and compressed at the same temperature. The HDA-to-LDA transformation occurs at $P \approx 0.6$ GPa. The qualitative agreement between (a) simulations and (b) experiments is evident.

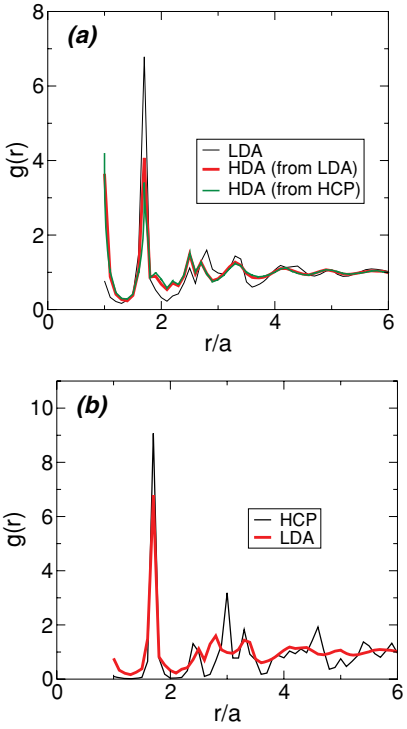

FIG. 8. (a) RDF $g(r)$ of LDA and HDA at $T = 0.1$, $P = 0.1$. The RDFs of HDA obtained upon compression of hcp (Fig. 2) and LDA (Fig. 7) are barely distinguishable. During the transformation, particles separated by a distance $r/a \approx 1.72 = b/a$, corresponding to the minimum of the pair potential interaction (Fig. 1), move closer to a separation distance $r/a \approx 1$, corresponding to the hard-core of the pair potential interaction. (b) Comparison of the RDFs of LDA and hcp at $T = 0.1$ and $P = 0.1$ showing that LDA is indeed amorphous. The RDF of LDA is almost constant for $r/a > 4$ while extrema are present in the RDF of hcp.

of recovered HDA) at low pressures. However, we can create a low-density amorphous solid by cooling the liquid.[19] We obtain LDA by quenching isochorically the equilibrium liquid along $L/a = 17.8$ at a rate $\approx 3 \times 10^{-4}\ q_T^0$ from $T = 0.4$ to $T = 0.1$, followed by equilibration of 10 000 time units at $T = 0.1$ and $P = 0.1$. At this rate, the entire cooling run lasts 1000 time units, which is about 30 times shorter than the time needed for the crystallization of hcp. A snapshot of the Jagla system corresponding to LDA at $T = 0.1$ and $P = 0.1$ is shown in Fig. 4(c). This glass obtained in simulations corresponds to the HGW produced in experiments. In the case of water, the slight difference in properties between ASW, HGW, and LDA is subtle, and all low-pressure glasses (HGW, ASW, and LDA) are collectively identified as LDA.[62] Thus, we will refer to the low-pressure glass obtained in simulations by quenching the liquid as LDA.

We follow the experimental protocol used in the discovery of the LDA-to-HDA transformation upon compression.[23] Specifically, we compress LDA at $T = 0.1$ from $P = 0.1$ to $P = 2.5$, as done in the simulations of Sec. III to study the PIA of the hcp crystal. The volume as function of pressure during the compression simulation is shown in Fig. 7(a). Figure 7(b) shows results from experiments on water where LDA ice is compressed at $T = 77$ K. The similarity between experiments and simulations is remarkable, as for both there is a sharp change in volume which corresponds to a transformation from LDA to HDA. The transformation resembles a first-order transition. Above and below the transformation pressure (≈ 0.7, simulations; ≈ 0.6 GPa, experiment), compression results in elastic deformation of the amorphous solids, i.e., volume, is proportional to pressure.

Figure 7 also shows the decompression curve of HDA for both experiment and simulation cases. In both cases, the LDA-to-HDA transformation is not reversible at the considered temperatures ($T = 0.1$, simulation; $T = 77$ K, experiment). In order to compare the structures of LDA and HDA, we show in Fig. 8(a) the corresponding RDFs at $P = 0.1$ and $T = 0.1$. For the case of HDA, we include the RDF obtained after compression of the hcp crystal (Fig. 2) and of LDA (Fig. 7). Both RDFs practically overlap, suggesting that the same amorphous solid results upon pressurization of the hcp crystal and LDA. Note that the same HDA is formed also in the water experiments by compressing ice I_h or LDA.[23]

The RDFs of both LDA and HDA display sharp maxima for small values of r. As r increases, the maxima in both RDFs decrease, indicating that these structures have no long-range order, i.e., LDA and HDA are indeed amorphous. Note that the structure of LDA is similar to that of the hcp crystal

[see Fig. 8(b)], but long-range order is observable only in the hcp crystal.

Figure 8(a) also shows that when going from LDA to HDA, particles separated by a distance $r/a = 1.72 = b/a$, corresponding to the minimum of the pair potential interaction [Fig. 1(a)], move closer so their new separation is $r/a = 1$, which corresponds to the hard-core part of the pair potential interaction. The structural changes in the LDA to HDA transformation are analogous to those observed in glassy water. For comparison, we note that in the case of water, LDA ice has a *local* structure similar to that of the low pressure ice (ice I_h), water molecules being surrounded by four nearest neighbors in a tetrahedral arrangement. When going from LDA to HDA, water molecules approach each other and, in the case of HDA, water molecules have an extra (fifth) neighbor located in the interstitial space between their first and second shell.[63]

V. TRANSFORMATIONS BETWEEN HIGH-DENSITY AND VERY-HIGH-DENSITY AMORPHOUS SOLIDS

A. Annealing high-density amorphous solid at high pressure

In 2001, experimental results on high-pressure glassy water raised the possibility that a third form of amorphous ice could exist,[40] called VHDA ice. VHDA was originally obtained by producing HDA (via PIA of ice I_h) at $T = 77$ K, followed by annealing (i.e., isobarically heating) to $T \approx 165$ K at $P \approx 1.1$ GPa. Experiments also show that VHDA does not convert back to HDA upon isobaric cooling back to $T = 77$ K.[40] Whether VHDA is a new phase of glassy water or a relaxed version of HDA is an unresolved question of considerable current interest.[38,45,64–68,70]

In this section we discuss whether the same phenomenology observed in the HDA-to-VHDA transformation in water is reproduced in our Jagla potential simulations. To do this, we first obtain HDA by compressing LDA at $T = 0.1$ to $P = 2.0$, as done in the simulation of Sec. IV B. Then, we heat HDA at $P = 2.0$ to a temperature just below the glass transition temperature. Figure 9(a) shows the evolution of volume upon heating HDA. For comparison, Fig. 9(b) shows analogous results obtained in water experiments, i.e., the change in volume when HDA ice is heated isobarically at $P = 1.1$ GPa (HDA was obtained by PIA of ice I_h at $T = 77$ K).[40] Results from simulations and experiments are qualitatively similar, indicating that HDA becomes denser upon annealing, resulting in a VHDA. In both cases, the HDA-to-VHDA transformation is smooth. In the simulation case, at $P = 2.0$ the glass transition is estimated to be at $T_g > 0.27$ [see Fig. 1(b)] so most of the volume changes shown in Fig. 9(a) correspond to the system being in the glass state.

As found in water experiments, simulations show that cooling VHDA back to the starting temperature does not result in HDA. Instead, the VHDA density continues to increase upon cooling [Fig. 9(a)]. As is found experimentally, VHDA can be decompressed at low temperature and recovered at $P \approx 0$. In our simulations, we decompress VHDA at $T = 0.1$ and recover VHDA at $T = 0.1$ and $P = 0.1$ (not shown). We find that at these conditions the density of VHDA ($V_{\mathrm{VHDA}} \approx 1.3$) is $\approx 10\%$ larger than the density of recovered HDA ($V_{\mathrm{HDA}} \approx 1.45$). Interestingly, at normal pressure and $T = 77$ K, the VHDA ice density is 9% larger than the HDA density.[40]

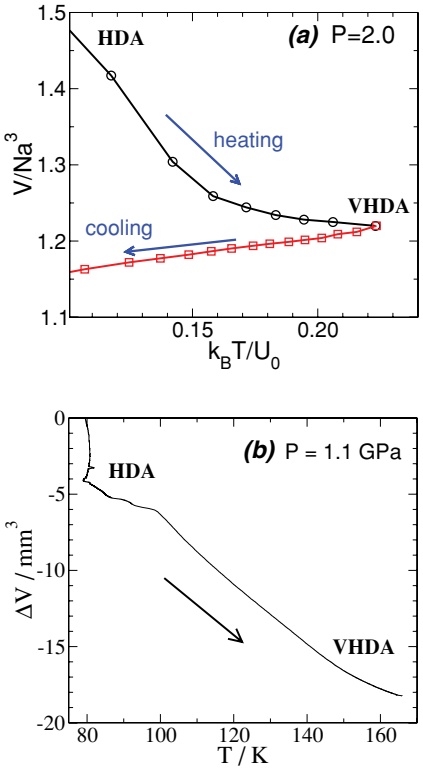

FIG. 9. HDA-to-VHDA transformation from (a) simulations and (b) experiments (from Ref. 40). In the simulation, the HDA configuration is obtained by compression of LDA at $T = 0.1$ to $P = 2$. VHDA is then obtained upon isobaric heating of HDA at $P = 2$. In the experiment, HDA is obtained upon compression of ice I_h at $T = 77$ K to $P = 1.1$ GPa. VHDA is then obtained upon isobaric heating of HDA at $P = 1.1$ GPa. Simulations and experiment show a similar HDA-to-VHDA transformation. This transformation is not reversible as indicated in (a), which is also in agreement with experiments.

Isobaric heating of recovered VHDA at $P = 0.1$ shows similar results to those of Fig. 5 for HDA. Upon heating, the glass transition is reached first and VHDA transforms to HDL (at $T \approx 0.25$). Upon further heating the HDL-spinodal line is crossed and HDL transforms to LDL (at $T \approx 0.3$). At $P = 0.1$ no VHDA-to-LDA transformation occurs.

Figure 10 shows the RDFs of HDA and VHDA at $P = 2.0$ and $T = 1.0$. The result of annealing HDA to form VHDA is to move particles from the second neighbor shell, $r/a \approx b/a = 1.72$ to the first shell, $r/a = 1$. No structural changes are observed beyond the second shell.

B. Isothermal compression of high-density amorphous solid

In experiments, VHDA ice can also be obtained upon compression of LDA ice at $T \approx 125$ K,[69] via a multistage transformation,[70–72] such as the sequence LDA → HDA → VHDA, where LDA transforms to HDA at $P \approx 0.5$ GPa, and HDA then transforms to VHDA at $P \approx 1$ GPa. The density versus pressure plot obtained in these experiments is

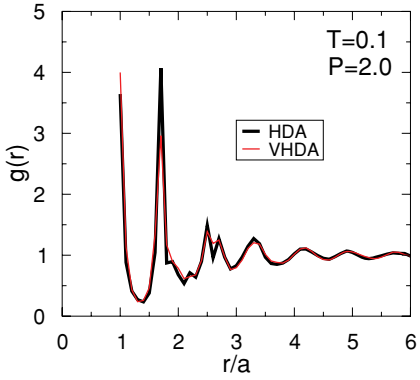

FIG. 10. Radial distribution functions of HDA and VHDA at $T = 0.1$ and $P = 2.0$. VHDA is obtained upon isobaric heating of HDA at $P = 2.0$ from $T = 0.1$ to $T = 0.24$ and cooled back to $T = 0.1$ (see Fig. 9).

shown in Fig. 11, where two density steps, one per transformation, can be identified. In our simulations, we only observe a single density step upon compressing LDA at $T = 0.1$ [Fig. 7(a)] corresponding to the LDA-to-HDA transformation. No density step associated with the HDA-VHDA transformation can be identified. In experiments, the density step associated with the HDA-VHDA transformation is very sensitive to the compression rate, and can only be observed at very slow rates.[69] A similar situation seems to occur in simulations. Standard MD simulations of water models,[45,67] such as SPC/E and TIP4P, do not reproduce the density step associated to the HDA-VHDA transformation upon compression. Such a density step has been reported from replica exchange MD in the *liquid* state (which allows simulation time scales much larger than those accessible in standard MD).[74] Therefore, the fast compression rates accessible in our MD computer simulations could be a reason for this discrepancy between simulations and experiments.

In order to explore the compression rate effects in our simulations, we age HDA at a temperature of $T = 0.2$ and for a range of seven different aging pressures $P_{age} = 0.5, 0.75, 1, 1.25, 1.5, 1.75$, and 2.0. All simulations

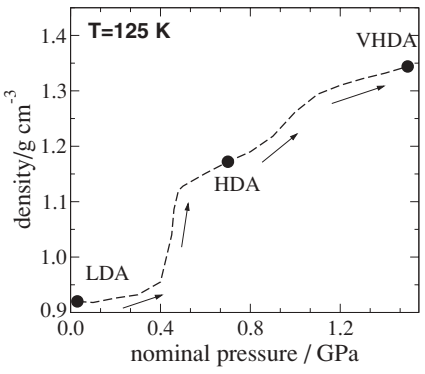

FIG. 11. Evolution of density with pressure from experiments where LDA ice is compressed at $T = 125$ K and slow compression rate of 20 MPa/min. Two density steps are observed. The first sharp step corresponds to the LDA-to-HDA transformation; the second, more gradual density step corresponds to the HDA-to-VHDA transformation. Adapted with permission from T. Loerting, C. G. Salzmann, K. Winkel, and E. Mayer, Phys. Chem. Chem. Phys. **8**, 2810 (2006). Copyright 2006, Royal Society of Chemistry.

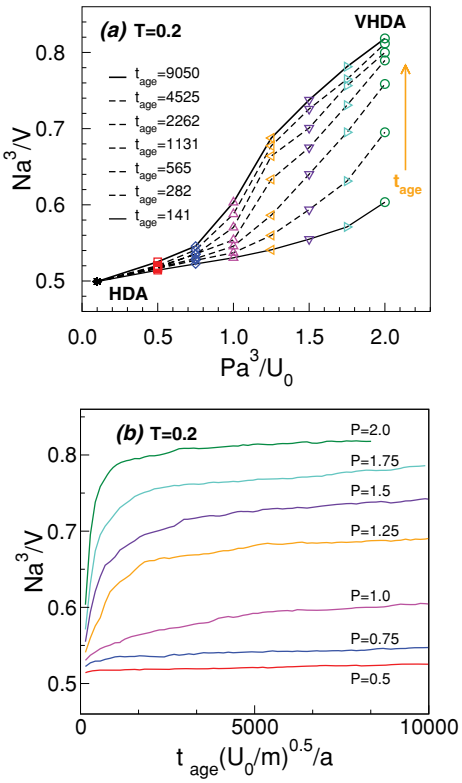

FIG. 12. (a) Effects of aging HDA in simulations. (b) Density vs aging time (t_{age}) as HDA is aged at fixed $T = 0.2$ and pressures (from bottom to top) $P_{age} = 0.5, 0.75, 1, 1.25, 1.5, 1.75$, and 2.0. Empty symbols in (a) indicate the system density at different t_{age} and $P = P_{age}$. We chose the symbol color to match the color of the corresponding $\rho(t_{age})$ curve shown in (b). Solid and dashed lines indicate the volume of the system as function of pressure, at fixed t_{age}. The $\rho(P)$ curves in (a) indicate that as t_{age} increases (see arrow), a density step develops at approximately $P > 0.7$, suggesting that if one could compress HDA at a much slower rate than the rate used in this work, one may be able to see a smooth density step between HDA and VHDA, analogous to the smooth density step shown in Fig. 11.

are started from the same configuration of HDA recovered at $T = 0.2$ and $P = 0.1$ [star symbol in Fig. 12(a)]. For each P_{age}, we take the HDA starting configuration and fix the barostat pressure to $P = P_{age}$, keeping $T = 0.2$. Figure 12(b) shows the evolution of the system density with aging time t_{age} for all the values of P_{age} studied. From these data we construct density versus P curves for different values of t_{age} [Fig. 12(a)]. The resulting $\rho(P)$ plots indicate that as t_{age} increases a density step develops at approximately $P > 0.7$. This suggests that if one could compress the Jagla LDA as shown in Fig. 7(a), but using a much slower rate than the rate used in this work, one may be able to see two density steps, in analogy with the density steps shown in Fig. 11.

C. Isothermal decompression of very-high-density amorphous solid

In water experiments, decompression of VHDA at $T = 77$ K does not result in HDA or LDA; a similar behavior is observed in simulations at $T = 0.1$. However, experiments indicate that decompression of VHDA at $T = 140$ K results in a slow VHDA-to-HDA transformation followed by a sharp HDA-to-LDA transformation.[64] Figure 13 shows the piston displacement upon decompressing different samples of

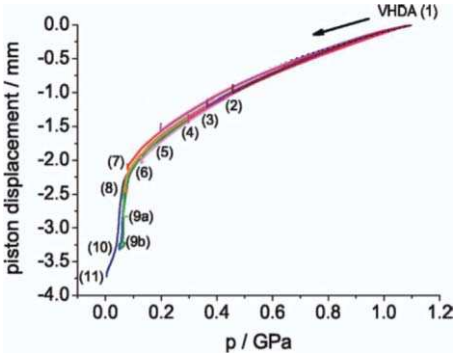

FIG. 13. Evolution of piston displacement with pressure from experiments where VHDA ice is compressed at $T = 140$ K with a slow decompression rate of 20 MPa/min. Numbers in parentheses indicate different samples taken for structural analysis. These structural studies (Ref. 64) indicate that VHDA is unchanged down to $P \approx 0.4$ GPa and transforms slowly to HDA in the range $P = 0.40$ to 0.06 GPa; HDA converts sharply to LDA at $P \approx 0.06$ GPa. Adapted with permission from K. Winkel, M. S. Elsaesser, E. Mayer, and T. Loerting, J. Chem. Phys. **128**, 044510 (2008). Copyright 2008, American Institute of Physics..

VHDA at $T = 140$ K. Structural analysis of the samples at different pressures[64] indicates that VHDA is unchanged down to $P \approx 0.4$ GPa, and transforms slowly to HDA in the range $P = 0.40$ to 0.06 GPa. Further decompression results in a sharp HDA-to-LDA transformation at $P \approx 0.06$ GPa.

Motivated by this finding, we decompress VHDA obtained by isobaric heating of HDA [see Fig. 9(a)] at $T = 0.2$ from $P = 2$. At the decompression rates accessible in simulations, we observe that VHDA transforms to LDL at negative pressures, without HDA formation. As discussed in the previous subsection, this could arise from the fast decompression rates accessible in our simulations, which are much larger than the experimental decompression rates. In order to test the effects of using slower decompression rates, we perform aging simulations as discussed in Sec. V B. Specifically, we take the same starting VHDA configuration, obtained at $T = 0.2$ and $P = 2$, and fix the pressure at seven different values $P_{\rm age} = 0.4$, 0.1, 0.0, −0.1, −0.20, −0.25, and −0.3, keeping $T = 0.2$. The evolution of the system density with aging time is shown in Fig. 14(b). From these data, we construct density versus pressure curves for different aging times $t_{\rm age}$; see Fig. 14(a).

Figure 14(a) shows that no transformation occurs at $P \geq 0.1$. At approximately $P \leq 0.0$, a VHDA-to-HDA transformation can be identified; the lower the pressure, the sooner HDA is formed. Within the aging times considered ($t_{\rm age} < 20,000$), it is found that at $P = -0.25$ and −0.3, further aging of HDA results in a HDA-to-LDL transformation, followed by crystallization of LDL into hcp crystal (not shown). In comparison to the VHDA-to-HDA transformation, the HDA-to-LDL transformation is very sharp. Therefore, these results suggest that if we could decompress the system at much slower rates than those we used, we could reproduce the experimental results of Ref. 64, i.e., a smooth transformation of VHDA to HDA over a wide pressure range, followed by a sharp HDA-to-LDL transformation. It is apparent from the simulations at $P < -0.25$ that the system is always trying to transform from VHDA to hcp; HDA and LDL being

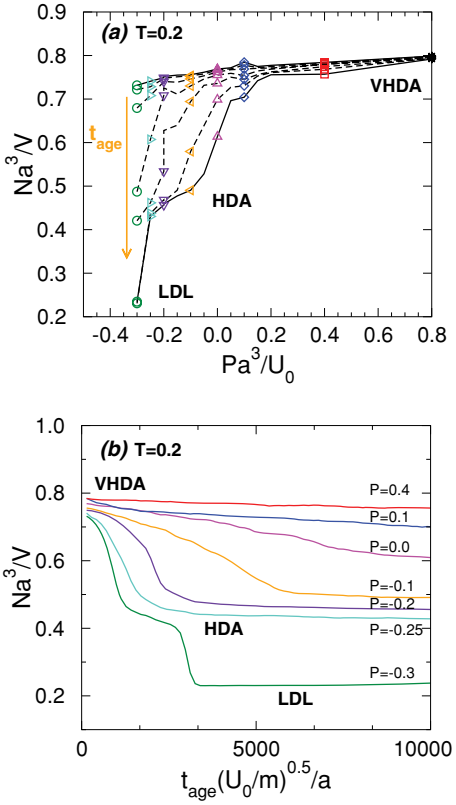

FIG. 14. (a) Simulations exploring the effects of aging VHDA. (b) Density vs normalized aging time ($t_{\rm age} = t(U_0/m)^{0.5}/a$) as VHDA is aged at fixed $T = 0.2$ and pressure (from bottom to top) $P_{\rm age} = -0.3$ (green), −0.25 (turquoise), −0.20 (violet), −0.10 (orange), 0.0 (pink), 0.1 (blue), and 0.4 (red). Empty symbols in (a) indicate the system volume at different $t_{\rm age}$ and $P = P_{\rm age}$. We choose the symbol color to match the color of the corresponding $V(t_{\rm age})$ curve shown in (b). Lines indicate the density of the system as function of pressure, at fixed $t_{\rm age}$. The $\rho(P)$ curves in (b) indicate that as $t_{\rm age}$ increases, a smooth transformation between VHDA and HDA develops at approximately $-0.2 < P < 0.2$, followed by a sharp HDA-to-LDL transformation at lower pressures. This suggests that if one could decompress VHDA at a much slower rate than those used in this work, one may be able to reproduce the results of the experiments shown in Fig. 13.

intermediate states that are less stable than hcp. Whether the system can be trapped in VHDA, HDA, or LDL upon decompression depends on the decompression rate and lowest pressure reached.

D. Differences between the HDA-LDA and VHDA-HDA transformations

An open question in the field of glassy water research is whether HDA and VHDA are separated by a first-order transition line, as is found experimentally for LDA and HDA.[39] We now address this question for the case of the Jagla pair potential. Since a first-order transition is accompanied by phase separation, we take snapshots of the system during the decompression-induced VHDA-to-HDA and HDA-to-LDA transformations at very low temperature and search for phase coexistence between the corresponding phases.

First we stretch HDA at constant temperature by simultaneously increasing all three dimensions of the simulation box (which contains $N = 1728$ particles) linearly with time, keeping periodic boundary conditions. We set

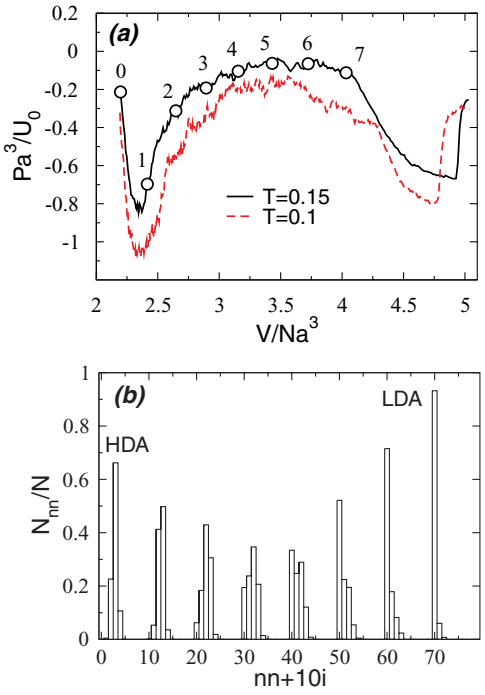

FIG. 15. (a) Pressure as function of volume per particle during isothermal stretching of HDA at $T = 0.15$ and $T = 0.1$. Solid circles indicate conditions numbered from $i = 0$ to $i = 7$ at which we compute histograms of number of nearest neighbors [panel (b)] and draw the snapshots of the system (Fig. 16). (b) Histograms of the number of particles with a certain number of nearest neighbors, nn. We shift x axis by $10i$ for the $i-$th set for clarity. One can see that the histogram becomes bimodal at the midpoint of the transformation when approximately half of the system transforms into LDA.

the relative velocity of the opposite sides of the box to be $7 \times 10^{-4}\sqrt{U_0/m}$. We measure the pressure as function of volume per particle [Fig. 15(a)]. Simultaneously we measure the number of nearest neighbors nn within a distance $1.3a$ from each particle and compute histograms of nn [Fig. 15(b)]. The distance $1.3a$ is selected to be the position of the first minimum of $g(r)$ for both LDA and HDA (Fig. 8). We also take snapshots of the system in which the particles with $nn \leq 1$ are colored white to indicate LDA and the rest of the particles are colored red (Fig. 16) to indicate HDA. This choice is based on the fact that the initial HDA system does not have particles with $nn \leq 1$ [Fig. 15(b)] while the final LDA phase does not have particles with $nn \geq 2$. The pressure first drops linearly with the increase of tensile strain but once HDA reaches its limit of stability, the pressure starts to increase. At this point the boundary between the high and low density states appears (Fig. 16). Soon the pressure stabilizes at a slightly negative value and remains constant until all HDA is transformed into a low density state (Fig. 16). During the entire transformation the boundary between HDA and the low density state can be clearly seen. Once HDA disappears, the pressure starts to drop again until the low density state reaches its limit of stability. At this point a cavity of gas appears in the system and the pressure starts to increase as the cavity grows. We can identify the low density state to be glass, because the pressure during the coexistence of two states fluctuates above the glass transition pressure of LDA for the particular temperature that we maintain during stretching. For example, in the simulation with $T = 0.15$, the pressure stays above $P = -0.2$, while the glass transition at this temperature occurs at $P = -0.5$ [see Fig. 1(b)]. In the simulation with $T = 0.10$, the pressure stays above $P = -0.5$, at which the glass transition is at $T = 0.15$. The size of the sample changes during stretching without particles of LDA being displaced relative to each other. The relative motion of particles occurs only at the interface with HDA. At both temperatures we can see clear phase segregation between the two states which is the evidence of the first-order phase transition between HDL and LDL, extrapolated into their glassy states.

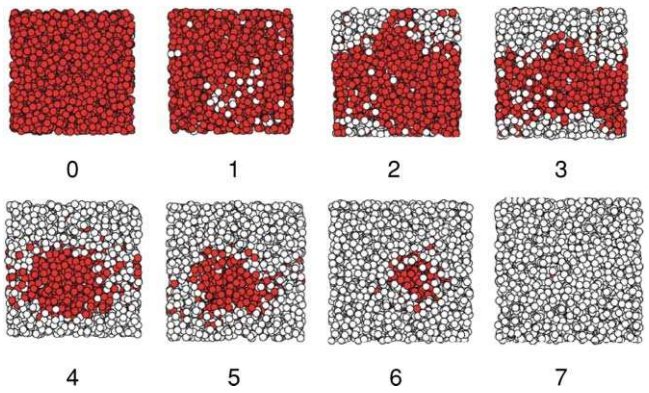

FIG. 16. Snapshots of the system during HDA stretching at $T = 0.15$ taken at the moments indicated by circles in Fig. 15(a). HDA particles are colored red, while LDA particles are colored white. One can see clear phase segregation between LDA and HDA phases at the stages of the transformation during which the pressure stays approximately constant. This feature is one of the main characteristics of the first order phase transition.

During VHDA stretching we measure pressure [Fig. 17(a)] and take snapshots of the system at different stages of stretching (Fig. 18) the same way as we did in the case of HDA stretching shown in Figs. 15 and 16. One can see that no significant segregation occurs at any stage of VHDA stretching. The particles which belong to LDA, HDA and VHDA are defined as follows. For each particle we measure the number of nearest neighbors nn within the distance $1.3a$ which corresponds to the first minimum of $g(r)$ for all three states (Figs. 8 and 10). If $nn \leq 1$ we ascribe the particle to the LDA state. If $2 \leq nn \leq 4$ we ascribe the particle to the HDA state, otherwise we ascribe the particle to the VHDA state. It is interesting to note that in the middle of the HDA-LDA transformation the distribution of nn is clearly bimodal with a minimum at $nn = 2$ [Fig. 15(b)], while during the VHDA-HDA transformation, the distribution of nn is always unimodal and as the transformation proceeds, the maximum of the distribution shifts to the left [Fig. 17(b)]. This is precisely what one might expect if the VHDA-to-HDA transformation were a relaxation effect. The results of Figs. 15(b), 16, 17(b), and 18 suggest that, at least for the Jagla pair potential, HDA and VHDA are not separated by a first-order transition but instead, the HDA-VHDA transformation can be interpreted as a relaxation effect.

VI. SUMMARY AND DISCUSSION

Water is one of the most studied substances that shows polyamorphism in the glassy state. In this work we study vitreous polyamorphism in a system of particles

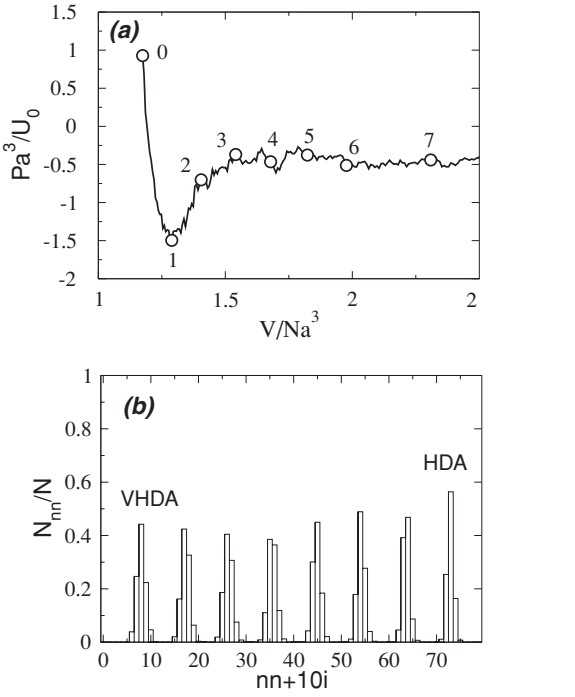

FIG. 17. (a) Pressure as function of volume per particle during isothermal stretching of VHDA at $T = 0.15$. Solid circles indicate conditions numbered from $i = 0$ to $i = 7$ at which we compute histograms of number of nearest neighbors [panel (b)] and draw the snapshots of the system (Fig. 18). (b) Histograms of the number of particles with a certain number of nearest neighbors, nn. We shift x axis by $10i$ for the $i-$th set for clarity. One can see that the histogram stays unimodal during the entire VHDA-HDA transformation.

interacting via a two-scale spherically-symmetric Jagla pair potential parametrized to reproduce the properties of liquid water. Our main focus is to investigate whether the known crystal-amorphous ice and amorphous ice-amorphous ice transformations observed in water can be reproduced by the same two-scale system used to describe liquid water.

Our results show striking parallels between glassy water experiments and the Jagla glass simulations. The low-pressure crystal-to-HDA transformation observed in our simulations is extremely sharp, resembling a first-order transition, as in the case of water experiments performed at $T = 77$ K.[39] Similarly, the LDA-to-HDA transformation obtained upon compression at $T = 77$ K is well reproduced by simulations. Note that the temperature used in our compression–decompression simulations is $T = 0.1$. This temperature, in physical units, is close to the temperature of the water experiments $T = 77$ K used as reference in this work. Using the value of U_0 for the case of water from Sec. II, we find that the simulation temperature is $T = 53$ K in physical units. It is not surprising, then, that both the crystal-to-HDA and LDA-to-HDA transformation are not reversible upon decompression in the simulations; indeed, experiments show that these transformations are not reversible.

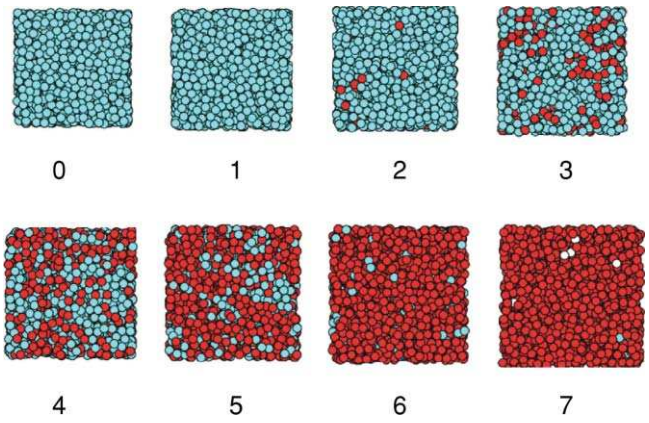

FIG. 18. Snapshots of the system during VHDA stretching at $T = 0.15$ taken at the moments indicated by circles in Fig. 17(a). VHDA particles are colored cyan, while HDA particles are colored red. There is no noticeable phase segregation of VHDA and HDA during the entire transformation.

Interestingly, the Jagla potential simulations show *quantitative* similarities to water experiments. Specifically, the ratio of the hcp crystal-to-HDA transition pressure to the LDA-to-HDA transformation pressure is 1.1 GPa/0.6 GPa= 1.83 [Figs. 2(b) and 7(b)]. The corresponding ratio for the simulation case is $1.35/0.7 = 1.93$ [Figs. 2(a) and 7(a)]. We also note that the transformation pressures obtained in simulations during both the crystal-HDA and LDA-to-HDA transformation are approximately one half of the corresponding pressures measured in water experiments if we convert them to physical values using $a = 2.7$ Å, $U_0 = 4.75$ KJ/mol. The hcp crystal-to-HDA transition at $T = 0.1$ (which corresponds to $T = 53$ K) is $P \approx 1.35$ in reduced units (U_0/a^3). Using the values of a and U_0 introduced in Sec. II for the case of water, we obtain $P = 0.54$ GPa. This value is roughly one half of the pressure obtained in water experiments (≈ 1.1 GPa) at $T = 77$ K. A similar analysis shows that the LDA-to-HDA transformation obtained in simulations, $P \approx 0.7$ in reduced units, corresponds to $P \approx 0.28$ GPa in physical units. This value is approximately one half of the corresponding value obtained in water experiments, ≈ 0.6 GPa. Quantitative agreement in absolute pressures is obtained if we use the picture described in Ref. 18, according to which one Jagla particle corresponds to two water molecules.

Since the pressure and temperature values for the different transitions in water can be estimated from the Jagla model simulations, it is natural to ask how the densities of the low-pressure crystal, LDA, and HDA compare with the corresponding predictions of Jagla LDA and Jagla HDA simulations. For the case of the low-pressure crystal, note that Fig. 2(a) indicates that $V \approx 3.8$ is the volume of the hcp crystal at $P = 0$ and $T = 0.1$ ($T = 53$ K and $P = 0$ GPa in physical units), corresponding to a density of $\rho = 0.80$ g/cm^3. This value is close to the densities of ice I_h at $T = 77$ K and $P = 1$ atm, $\rho = 0.94$ g/cm^3 (Ref. 23). For the case of LDA, we obtain a density of 0.91 g/cm^3 at $T = 53$ K and $P = 0$ GPa ($P = 0$, $T = 0.1$, and $V \approx 3.35$ in reduced units [see Fig. 7(a)]. This value is close to the corresponding experimental density of Jagla LDA, 0.94 g/cm^3 at $T = 77$ K and $P = 1$ bar. The density of Jagla HDA indicated in Fig. 2(a) at $P = 2$ and $T = 0.1$ (corresponding to $T = 53$ K and $P = 1.6$ GPa in water experiments), is $\rho = 2.17$ g/cm^3. This value is larger than the density of Jagla HDA measured at $T = 77$ K and $P \approx 1.75$ GPa, i.e., $\rho = 1.42$ g/cm^3.[23] This difference in density remains at low pressure. Jagla HDA density at $P = 0$ and $T = 0.1$ is $\rho = 2.03$ g/cm^3 (corresponding to $T = 53$ K and $P = 0$ GPa in water experiments) while the density of

HDA measured at $T = 77$ K and $P = 1$ bar is $\rho = 1.17$ g/cm^3 (Ref. 23). The discrepancy between HDA density and the Jagla HDA density agrees with the discrepancies in the slope of the HDL-LDL coexistence line, which is negative for water but is positive for the Jagla potential indicating that the entropy of HDL is smaller than that of LDL. This entropy decrease is associated with dramatic volume loss.

We find that the HDA-to-VHDA transformation can be identified in our simulations upon isobaric heating of HDA at high pressure. The volume changes observed in simulations upon heating are similar to those reported in experiments.[23,40] With the compression and decompression rates accessible in simulations, we were not able to reproduce the HDA-VHDA transformations observed in glassy water upon compression and decompression. However, our aging simulations of HDA and VHDA at different pressures indicate that HDA and VHDA can be interconverted with pressure with slower compression/decompression rates than those used in this work. Also, we could not identify for the Jagla model VHDA-to-HDA or HDA-to-LDA transformations upon heating the glasses at positive but low pressures, but only at negative pressure (or, in the case of the HDA-LDA transition, inserting a free surface).

Our results confirm that the Jagla potential appears to exhibit many of the liquid-phase anomalies of water and, moreover, that simple isotropic particles can exhibit complex behavior observed in the glass state. The present model is unusual since, contrary to what occurs in most monoatomic model systems, crystallization can be avoided on simulation time scales, allowing the exploration of polyamorphism below the glass transition. The Jagla model thus provides a particularly useful tool for exploration of glassy polyamorphism not only for water, but also for systems with isotropic interactions, such as glassy metals.[31]

ACKNOWLEDGMENTS

We thank C. A. Angell for enlightening discussions and suggestions in all stages of this research. L.X. thanks the World Premier International Research Center Initiative (WPI Initiative) and the Grand-in-Aid for Young Scientists (B), MEXT, Japan. L.X. also thanks the allocation of computation time on SGI Altix 3700B2 at the Advanced Fluid Information Research Center, Institute of Fluid Science, Tohoku University. N.G. acknowledges financial support from CUNY, PSC-CUNY-40 award. S.V.B. thanks the Office of the Academic Affairs of Yeshiva University for funding the Yeshiva University high-performance computer cluster and acknowledges the partial support of this research through the Dr. Bernard W. Gamson Computational Science Center at Yeshiva College. P.G.D. and H.E.S. gratefully acknowledge the support of the National Science Foundation (Collaborative Research in Chemistry Awards CHE-0908265 to P.G.D., and CHE-0404673 and CHE-0908218 to H.E.S.).

[1] See, e.g., P. G. Debenedetti, *Metastable Liquids: Concepts and Principles* (Princeton University, Princeton, NJ, 1996).
[2] P. G. Debenedetti and H. E. Stanley, Phys. Today **56**, 40 (2003); P. G. Debenedetti, J. Phys. Condens. Matter. **15**, R1669 (2003).
[3] I. Saika-Voivod, P. H. Poole, and F. Sciortino, Nature (London) **412**, 514 (2001).
[4] For simulations, see S. Sastry and C. A. Angell, Nature Mater. **2**, 739 (2003); P. Ganesh and M. Widom, Phys. Rev. Lett. **102**, 075701 (2009). For experiments, see M. Beye, F. Sorgenfrei, W. F. Schlotter, W. Wurth, and A. Föhlisch, Proc. Nat. Acad. Sci. U.S.A. **107**, 16772 (2010); and the accompanying work S. Sastry, Proc. Nat. Acad. Sci. U.S.A. **107**, 17063 (2010).
[5] P. C. Hemmer and G. Stell, Phys. Rev. Lett. **24**, 1284 (1970).
[6] G. Stell and P. C. Hemmer, J. Chem. Phys. **56**, 4274 (1972).
[7] For a recent review, see, e.g., S. V. Buldyrev, G. Malescio, C. A. Angell, N. Giovambattista, S. Prestipino, F. Saija, H. E. Stanley, and L. Xu, J. Phys. Condens. Matter **21**, 504106 (2009).
[8] E. A. Jagla, J. Chem. Phys. **111**, 8980 (1999); Phys. Rev. E **63**, 061501 (2001).
[9] M. R. Sadr-Lahijany, A. Scala, S. V. Buldyrev, and H. E. Stanley, Phys. Rev. Lett. **81**, 4895 (1998); M. R. Sadr-Lahijany, A. Scala, N. Giovambattista, S. V. Buldyrev, and H. E. Stanley, Phys. Rev. E **63**, 041202 (2001).
[10] T. Head-Gordon and F. H. Stillinger, J. Chem. Phys. **98**, 3313 (1993).
[11] A. B. de Oliveira, P. A. Netz, and M. C. Barbosa, Europhys. Lett. **85**, 36001 (2009); P. A. Netz, S. V. Buldyrev, M. C. Barbosa, and H. E. Stanley, Phys. Rev. E **73**, 061504 (2006); A. de Oliveira, E. Salcedo, C. Chakravarty, and M. Barbosa, J. Chem. Phys. **132**, 234509 (2010); A. B. de Oliveira, E. B. Neves, C. Gavazzoni, J. Z. Paukowski, P. A. Netz, and M. C. Barbosa, J. Chem. Phys. **132**, 164505 (2010).
[12] Z. Yan, S. V. Buldyrev, N. Giovambattista, P. G. Debenedetti, and H. E. Stanley, Phys. Rev. E **73**, 051204 (2006); see also M. Canpolat, F. W. Starr, M. R. Sadr-Lahijany, A. Scala, O. Mishima, S. Havlin, and H. E. Stanley, Chem. Phys. Lett. **294**, 9 (1998) for calculations of the effects of two length scales on the existence of an LLCP.
[13] Z. Yan, S. V. Buldyrev, P. Kumar, N. Giovambattista, P. G. Debenedetti, and H. E. Stanley, Phys. Rev. E **76**, 051201 (2007).
[14] G. Franzese, G. Malescio, A. Skibinsky, S. V. Buldyrev, and H. E. Stanley, Nature (London) **409**, 692 (2001); G. Franzese, G. Malescio, A. Skibinsky, S. V. Buldyrev, and H. E. Stanley, Phys. Rev. E **66**, 051206 (2002); G. Malescio, G. Franzese, A. Skibinsky, S. V. Buldyrev, and H. E. Stanley, Phys. Rev. E **71**, 061504 (2005); E. Lascaris, G. Malescio, S. V. Buldyrev, and H. E. Stanley, Phys Rev. E **81**, 031201 (2010); G. Franzese, J. Mol. Liq. **136**, 267 (2007).
[15] A. B. de Oliveira, P. Vilaseca and G. Franzese, P. A. Netz, and M. C. Barbosa, J. Chem. Phys. **128**, 064901 (2008); P. Vilaseca and G. Franzese, J. Chem. Phys. **133**, 084507 (2010); J. Non-Crystalline Sol. **357**, 419 (2011).
[16] P. T. Cummings and G. Stell, Mol. Phys. **43**, 1267 (1981).
[17] Z. Yan, S. V. Buldyrev, N. Giovambattista, and H. E. Stanley, Phys. Rev. Lett. **95**, 130604 (2005).
[18] Z. Yan, S. V. Buldyrev, P. Kumar, N. Giovambattista, and H. E. Stanley, Phys. Rev. E **77**, 042201 (2008).
[19] L. Xu, S. V. Buldyrev, N. Giovambattista, C. A. Angell, and H. E. Stanley, J. Chem. Phys. **130**, 054505 (2009).
[20] V. Molinero and E. B. Moore, J. Phys. Chem. B **113**, 4008 (2009); E. B. Moore and V. Molinero, J. Chem. Phys. **130**, 244505 (2009); L. Xu and V. Molinero, J. Phys. Chem. B **114**, 7320 (2010).
[21] H. M. Gibson and N. B. Wilding, Phys. Rev. E **73**, 061507 (2006).
[22] L. Xu, S. V. Buldyrev, C. A. Angell, and H. E. Stanley, Phys. Rev. E **74**, 031108 (2006); L. Xu, F. Mallamace, Z. Yan, F. W. Starr, S. V. Buldyrev, and H. E. Stanley, Nat. Phys. **5**, 565 (2009).
[23] O. Mishima, L. D. Calvert, and E. Whalley, Nature (London) **310**, 393 (1984); Nature (London) **314**, 76 (1985).
[24] For a review of experiments on liquid and glassy water, see, e.g., O. Mishima and H. E. Stanley, Nature (London) **396**, 329 (1998).
[25] P. H. Poole, F. Sciortino, U. Essmann, and H. E. Stanley, Nature (London) **360**, 324 (1992); P. H. Poole, U. Essmann, F. Sciortino, and H. E. Stanley, Phys. Rev. E **48**, 4605 (1993).
[26] O. Mishima and H. E. Stanley, Nature (London) **392**, 164 (1998).
[27] O. Mishima, J. Chem. Phys. **133**, 144503 (2010)..
[28] Y. Zhang, A. Faraone, W. A. Kamitakahara, K.-H. Liu, C.-Y. Mou, J. B. Leo, and S.-H. Chen, Proc. Natl. Acad. Sci (in press).
[29] Y. Katayama, T. Mizutani, W. Utsumi, O. Shimomura, M. Yamakata, and K. Funakosh, Nature (London) **403**, 170 (2000).
[30] M. H. Bhat, V. Molinero, E. Soignard, V. C. Solomon, S. Sastry, J. L. Yarger, and C. A. Angell, Nature (London) **448**, 787 (2007).
[31] H. W. Sheng, H. Z. Liu, Y. Q. Cheng, J. Wen, P. L. Lee, W. K. Luo, S. D. Shastry, and E. Ma, Nature Mater. **6**, 192 (2007).

[32]R. Kurita, Y. Shinohara, Y. Amemiya, and H. Tanaka, J. Phys. Condens. Matter **19**, 152101 (2007).
[33]S. Aasland and P. F. McMillan, Nature (London) **369**, 633 (1994).
[34]M. C. Wilding, M. Wilson, and P. F. McMillan, Chem. Soc. Rev. **35**, 964 (2006).
[35]A. Barnes, L. B. Skinner, P. S. Salmon, A. Bytchkov, I. Pozdnyakova, T. O. Farmer, and H. E. Fisher, Phys. Rev. Lett. **103**, 225702 (2009).
[36]P. F. McMillan, J. Mater. Chem. **14**, 1506 (2004).
[37]L. Xu, P. Kumar, S. V. Buldyrev, S.-H. Chen, P. H. Poole, F. Sciortino, and H. E. Stanley, Proc. Natl. Acad. Sci. U.S.A. **102**, 16558 (2005).
[38]T. Loerting and N. Giovambattista, J. Phys. Condens. Matter **18**, R919 (2006).
[39]O. Mishima, J. Chem. Phys. **100**, 5910 (1994).
[40]T. Loerting, C. Salzmann, I. Kohl, E. Mayer, and A. Hallbrucker, Phys. Chem. Chem. Phys. **3**, 5355 (2001).
[41]D. C. Rapaport, *The Art of Molecular Dynamics Simulation* (Cambridge University Press, Cambridge, 1995).
[42]For a review, see S. V. Buldyrev, "Application of discrete molecular dynamics to protein folding," in *Proceedings of the Sitges Conference: Aspects of Physical Biology,* Lecture Notes in Physics, edited by G. Franzese and M. Rubi (Springer-Verlag, Berlin, 2008), pp. 97–132.
[43]S. V. Buldyrev and H. E. Stanley, Physica A **330**, 124 (2003).
[44]N. Giovambattista, C. A. Angell, F. Sciortino, and H. E. Stanley, Phys. Rev. Lett. **93**, 047801 (2004).
[45]R. Martonák, D. Donadio, and M. Parrinello, J. Chem. Phys. **122**, 134501 (2005).
[46]J. Hemley, A. P. Jephcoat, H. K. Mao, L. C. Ming, and M. H. Manghnani, Nature (London) **334**, 52 (1988).
[47]Q. Williams and R. Jeanloz, Nature (London) **338**, 413 (1989).
[48]G. Yu. Machavariani, G. Kh. Rozenberg, M. P. Pasternak, O. Naaman, and R. D. Taylor, Physica B **265**, 105 (1999).
[49]H. Luo and A. L. Ruoff, Phys. Rev. B **48**, 569 (1993).
[50]M. P. Pasternak, R. D. Taylor, M. B. Kruger, R. Jeanloz, J.-P. Itie, and A. Polian, Phys. Rev. Lett. **72**, 2733 (1994).
[51]E. Gregoryanz, A. F. Goncharov, R. J. Hemley, and H. K. Mao, Phys. Rev. B **64**, 052103 (2001).
[52]W. Williamson and S. A. Lee, Phys. Rev. B **44**, 9853 (1991).
[53]M. B. Kruger and C. Meade, Phys. Rev. B **55**, 1 (1997).
[54]M. C. Bellissent-Funel, L. Bosio, A. Hallbrucker, E. Mayer, and R. Sridi-Dorbez, J. Chem. Phys. **97**, 1282 (1992).
[55]E. F. Burton and W. F. Oliver, Proc. R. Soc. London, Ser. A **153**, 166 (1935).
[56]E. Mayer, J. Appl. Phys. **55**, 663 (1985).
[57]D. T. Bowron, J. L. Finney, A. Hallbrucker, I. Kohl, T. Loerting, E. Mayer, and A. K. Soper, J. Chem. Phys. **125**, 194502 (2006).
[58]G. P. Johari, A. Hallbrucker, and E. Mayer, Nature (London) **330**, 552 (1987).
[59]S. K. Deb, M. Wilding, M. Somayazuluik, and P. F. McMillan, Nature (London) **306**, 845 (2004).
[60]R. Kurita and H. Tanaka, Science **403**, 170 (2000).
[61]O. Mishima, K. Takemura, and K. Aoki, Science **254**, 406 (1991).
[62]P. G. Debenedetti, J. Phys. Condens. Matter **15**, R1669 (2003).
[63]J. L. Finney, A. Hallbrucker, I. Kohl, A. K. Soper, and D. T. Bowron, Phys. Rev. Lett. **88**, 225503 (2002).
[64]K. Winkel, M. S. Elsaesser, E. Mayer, and T. Loerting, J. Chem. Phys. **128**, 044510 (2008).
[65]K. Winkel, M. Bauer, E. Mayer, M. Seidl, M. S. Elsaesser, and T. Loerting, J. Phys. Condens. Matter **20**, 494212 (2008).
[66]D. D. Klug, Nature (London) **420**, 749 (2002).
[67]N. Giovambattista, H. E. Stanley and F. Sciortino, Phys. Rev. Lett. **94**, 107803 (2005); Phys. Rev. E **72**, 031510 (2005).
[68]R. Martonák, D. Donadio, and M. Parrinello, Phys. Rev. Lett. **92**, 225702 (2004).
[69]T. Loerting, W. Schustereder, K. Winkel, C. G. Salzmann, I. Khol, and E. Mayer, Phys. Rev. Lett. **96**, 025702 (2006).
[70]O. Mishisma and Y. Suzuki, Nature (London) **384**, 546 (1996); Nature (London) **419**, 599 (2002).
[71]M. M. Koza, B. Geil, K. Windel, C. Köhler, F. Czeschka, M. Scheuermann, H. Schober, and T. Hansen, Phys. Rev. Lett. **94**, 125506 (2005).
[72]C. A. Tulk, R. Hart, D. D. Klug, C. J. Benmore, and J. Neuefeind, Phys. Rev. Lett. **97**, 115503 (2006).
[73]T. Loerting, C. G. Salzmann, K. Winkel, and E. Mayer, Phys. Chem. Chem. Phys. **8**, 2810 (2006).
[74]D. Paschek, A. Rüppert, and A. Geiger, ChemPhysChem **9**, 2737 (2008).